AIP | The Journal of Chemical Physics

Dynamics of dipole- and valence bound anions in iodide-adenine binary complexes: A time-resolved photoelectron imaging and quantum mechanical investigation

Anne B. Stephansen, Sarah B. King, Yuki Yokoi, Yusuke Minoshima, Wei-Li Li, Alice Kunin, Toshiyuki Takayanagi, and Daniel M. Neumark

Citation: The Journal of Chemical Physics **143**, 104308 (2015); doi: 10.1063/1.4929995
View online: http://dx.doi.org/10.1063/1.4929995
View Table of Contents: http://scitation.aip.org/content/aip/journal/jcp/143/10?ver=pdfcov
Published by the AIP Publishing

THE JOURNAL OF CHEMICAL PHYSICS **143**, 104308 (2015)

Dynamics of dipole- and valence bound anions in iodide-adenine binary complexes: A time-resolved photoelectron imaging and quantum mechanical investigation

Anne B. Stephansen,[1] Sarah B. King,[2] Yuki Yokoi,[3] Yusuke Minoshima,[3] Wei-Li Li,[2]
Alice Kunin,[2] Toshiyuki Takayanagi,[3] and Daniel M. Neumark[2,4,a)]
[1]*Department of Chemistry, University of Copenhagen, Universitetsparken 5, DK-2100 København Ø, Denmark*
[2]*Department of Chemistry, University of California, Berkeley, California 94720, USA*
[3]*Department of Chemistry, Saitama University, 255 Shimo-Okubo, Sakura-ku, Saitama City, Saitama 338-8570, Japan*
[4]*Chemical Sciences Division, Lawrence Berkeley National Laboratory, Berkeley, California 94720, USA*

(Received 16 June 2015; accepted 21 August 2015; published online 9 September 2015)

Dipole bound (DB) and valence bound (VB) anions of binary iodide-adenine complexes have been studied using one-color and time-resolved photoelectron imaging at excitation energies near the vertical detachment energy. The experiments are complemented by quantum chemical calculations. One-color spectra show evidence for two adenine tautomers, the canonical, biologically relevant A9 tautomer and the A3 tautomer. In the UV-pump/IR-probe time-resolved experiments, transient adenine anions can be formed by electron transfer from the iodide. These experiments show signals from both DB and VB states of adenine anions formed on femto- and picosecond time scales, respectively. Analysis of the spectra and comparison with calculations suggest that while both the A9 and A3 tautomers contribute to the DB signal, only the DB state of the A3 tautomer undergoes a transition to the VB anion. The VB anion of A9 is higher in energy than both the DB anion and the neutral, and the VB anion is therefore not accessible through the DB state. Experimental evidence of the metastable A9 VB anion is instead observed as a shape resonance in the one-color photoelectron spectra, as a result of UV absorption by A9 and subsequent electron transfer from iodide into the empty π-orbital. In contrast, the iodide-A3 complex constitutes an excellent example of how DB states can act as doorway state for VB anion formation when the VB state is energetically available. © *2015 AIP Publishing LLC*. [http://dx.doi.org/10.1063/1.4929995]

I. INTRODUCTION

Interactions between nucleic acid constituents and low-energy electrons can result in transient negative anions with the potential consequence of irreversible DNA lesions.[1–10] DNA strand breaks have been observed to occur at electron energies well below the ionization threshold of any of the DNA moieties,[3,7] and this intriguing result has motivated numerous studies on the damage mechanism. Cleavage is believed to occur by dissociative electron attachment (DEA),[5–15] where the electron initially is captured by one of the DNA components. If the resulting anion has a sufficiently long autodetachment lifetime, it can dissociate into anionic and neutral fragments.[6] The nucleobases[7,8,10,11,13,14] and phosphate units[16,17] have been suggested as potential electron trapping sites due to their low-energy π* orbitals.[15] Electron scattering experiments have shown that all DNA bases in the gas phase exhibit shape resonances below their ionization energies,[1] and DEA experiments reveal that attachment of low energy electrons can result in hydrogen loss at the nitrogen atoms that link the base to the sugar-phosphate.[6,18–23] Theoretical studies predict that strong electronic coupling facilitates transfer of the electron from the base to the sugar-phosphate units, where cleavage most efficiently occurs.[11,14,15,24] While the π* orbitals of the nucleobases appear to be the primary electron trapping sites, the mechanism for the electron capture is still not fully understood.[6,8,25,26] Here, following up on previous work on gas phase, binary anion clusters,[27–31] we focus on the initial electron capture dynamics by the nucleobase adenine complexed with iodide, the electron donor, using femtosecond time-resolved photoelectron imaging (PEI).[27–31] In these experiments, an UV pump pulse induces electron transfer from iodide to the base and is followed by an IR pulse that detaches the electron, thus probing how the base accommodates the electron,

$$I^- \cdots Base \xrightarrow{h\nu_{pump}} I \cdots Base^- \xrightarrow{\Delta t, h\nu_{probe}} I \cdots Base + e^-\left(eKE = h\nu_{probe} - eBE\right). \quad (1)$$

A key issue in electron/nucleobase interactions is the role of dipole-bound (DB) and valence-bound (VB) states of the nucleobase anion. All nucleobases have dipole moments larger than ≈2-2.5 D and can, in principle, bind an electron by electrostatic charge-dipole interactions; in such DB anions, the electron resides in a highly diffuse, anisotropic orbital largely outside the molecular framework.[32–35] In DEA experiments, the DB anions have been proposed to act as doorway states to the formation of a conventional VB anion,[36,37] in which the

---

[a)]Author to whom correspondence should be addressed. Electronic mail: dneumark@berkeley.edu

excess electron is located in an antibonding molecular orbital. However, the role of the DB anion as a precursor state for VB anion formation has not yet been proven.

Previous investigations from our laboratory examined anion dynamics in photoexcited binary complexes of iodide with nitromethane, acetonitrile,[30] uracil,[27–29,31] and thymine.[27,28,31] Acetonitrile and nitromethane were examined as model systems; while acetonitrile only supports a stable DB anion, nitromethane exhibits both DB and VB anions and demonstrates a complete and efficient DB to VB state transition.[30] Uracil and thymine display more complex anion dynamics due to a combination of effects. These include stronger interactions between iodide and the bases, nearly iso-energetic DB and VB anions, and non-negligible barriers for their inter-conversion.[27,29,31,38–40] For uracil and thymine, experiments were performed in two different pump photon energy regimes: near the cluster, vertical detachment energy (VDE, defined as the difference in energy between the neutral and the anion at the equilibrium geometry of the anion) and several hundred meV above the VDE.[27–29,31] While DB anions were observed only in the low-energy regime, VB anions were observed at all excitation energies. It was concluded that the formation mechanism depends on the energy regime. At the higher energies, VB anions are accessed directly from the I^-·base ground state complexes and formed in a vibrationally excited state; the resulting VB anions of uracil and thymine have lifetimes of just a few picoseconds with respect to autodetachment. Near the VDE, VB anions are formed through a precursor state, and the VB anions exhibit lifetimes an order of magnitude larger than in the higher excitation energy regime. Whether the DB anion acts as doorway state in the low-energy regime was not fully clear, since no matching decay and rise components of, respectively, the DB and VB states were observed. However, the DB states (when present) always appeared before the VB state, and the DB anion and/or dipole scattering states of the neutral continuum[41,42] appear to be the most plausible gateways for VB anion formation near the VDE.[31]

Thus far, the DB and VB anions of the pyrimidine bases uracil and thymine have been studied more extensively than the anions of cytosine and the purine bases guanine and adenine, the last being the current focus. The dipole moment of the most stable and biologically relevant adenine tautomer A9 (Scheme 1(a)) is 2.5-2.8 D[43,44] which is near the minimum dipole moment known to support a DB anion (2.2-2.5 D).[32–34] The result is a smaller electron binding energy for the DB anion of A9 compared to uracil and thymine (μ ≈ 4.2 D).[45,46] While signatures of the A9 DB state were observed in Rydberg Electron Transfer (RET) experiments, yielding an electron affinity (EA, defined as the difference in energy between the neutral and anion ground states) of +11-12 meV,[43] a photoelectron spectrum of the DB anionic state has, to our knowledge, never been measured. Photoelectron spectra of gas phase adenine VB anions have been reported, but the authors concluded that the observed peaks originate from a range of different adenine tautomers,[47,48] and the literature reports no experimental measurements of the VDE of the A9 VB state. Theoretically, the VDE of the A9 VB anion has been estimated to be +0.03 eV.[49] Experimental investigations involving RET,[50] DEA,[9,18,20] and electron transmission spectroscopy[1,51] find a range of +(0.45-0.54) eV for vertical electron attachment to the A9 valence orbital. High-level energy calculations—albeit predicting very dispersed values depending on the calculation method—agree that the VB anion of A9 is not adiabatically bound.[52] These results suggest that the VB anion of A9 is adiabatically unstable with respect to the neutral and only weakly bound vertically if at all. This differs from the situation for uracil and thymine, where the VB anions are predicted to be at least vertically bound, while it is unclear whether the VB anions are adiabatically bound with respect to the neutral in the gas phase. Upon complexation to a proton donor (water,[53] methanol,[50] and formic acid[54]), the A9 VB anion becomes observable in photoelectron spectroscopy, either due to electrostatic interactions and/or the proton-donating abilities of the complexed species stabilizing the VB anion. Experimental[53] and theoretical[55] works on adenine-water clusters suggest that it takes up to three or four water molecules to make the A9 VB anion adiabatically bound, and for smaller clusters, the anion is assumed only to be stable with respect to vertical detachment.

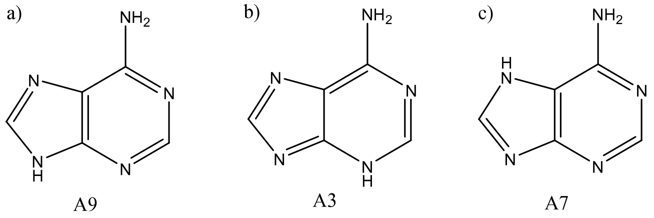

SCHEME 1. The three most stable tautomers of adenine.

While the previous studies indicate that the gas phase A9 VB anion is higher in energy than the corresponding neutral, the Bowen group has reported evidence of both vertically and adiabatically stable VB anions of other adenine tautomer(s), possibly an enamine/imine form, that was suspected to be formed due to harsh source conditions.[47] It is well-known that adenine has several stable tautomers including both amine and enamine/imine forms, with the amine forms A9, A7, and A3 (Scheme 1) being lowest in energy.[49] A9 is predicted to be the only tautomer present at significant amounts in the gas phase, but A3 is estimated to be preferentially stabilized in small clusters,[44] and A7 attains a ≈20% abundance in aqueous solutions due to its significant dipole moment.[44,56] While both A3 and A7 exhibit dipole moments (approximately 4.7 D and 6.8 D, respectively[44]) large enough to support DB anions,[35,57] relatively little work has focused on the anions of these tautomers. To our knowledge, no experimental data exist on the DB anions of A3 and A7, but the Adamowicz group addressed the DB state of A7 theoretically and found an EA of +60-110 meV depending on the level of theory.[57] Raczyńska *et al.* investigated the VB anions of adenine tautomers theoretically and estimated adiabatic EAs (AEAs) of −170 meV and +130 meV for A7 and A3, respectively, suggesting that only A3 forms stable VB anions.[49]

Here, we investigate the anions of adenine and the photo-induced iodide-adenine dynamics in the energy regime near the cluster VDE using both one-color and femtosecond time-resolved PEI of iodide-adenine (I^-·A) complexes. The experimental work is combined with quantum chemical calculations that consider potential contributions from the three adenine tautomers in Scheme 1. One-photon PEI shows evidence of both the $I^-{\cdot}A9$ and $I^-{\cdot}A3$ complexes exhibiting VDEs of 3.96 eV and 4.11 eV, respectively. Indications of an unbound A9 VB anion are observed at detachment photon energies overlapping with the A9 UV absorption band and appear as a photon-energy-invariant resonance. We tentatively ascribe this resonance to UV absorption by A9 followed by electron transfer from iodide into an empty A9 valence orbital, forming an A9 VB anion that autodetaches. Time-resolved experiments show that photoexcitation of $I^-{\cdot}A9$ and $I^-{\cdot}A3$ forms DB anions, but the A9 DB anion is formed in a narrower range of excitation energies than the A3 DB anion. The A3 DB state decays into a VB anion, and the transition appears to be efficient and complete at all examined energies, consistent with our theoretically predicted potential energy surfaces for the dipole-to-valence transition of the A3 anion. The work presented here complements time-resolved experiments on electronically excited adenine in the gas phase and in solution.[58–60]

II. EXPERIMENTAL

A. Photoelectron spectroscopy

The time-resolved photoelectron imaging spectrometer has been described in detail elsewhere.[61,62] Iodide-adenine clusters were formed by flowing 50 psig neon over a reservoir containing iodomethane and through a pulsed (500 Hz) Even-Lavie valve containing adenine (purchased from Sigma-Aldrich, purity ≥99%) heated to 210 °C. The mixture was adiabatically expanded into vacuum and passed through a ring-filament ionizer. The resulting ions were mass-separated in a Wiley-McLaren mass spectrometer, and only clusters of the desired mass were allowed to enter the laser interaction region. NMR spectra were conducted before and after heating to verify that adenine does not decompose into imine/enamine tautomeric forms. Due to the structural similarity between A9, A7, and A3, we cannot rule out from the NMR data whether A3 and A7 are formed in the source as a result of heating the sample.

The femtosecond (fs) laser system consists of a KM Labs Griffin oscillator and a Dragon amplifier and generates pulses centered at 1.58 eV (790 nm) with a 1 kHz repetition rate. In the time-resolved experiments, the excitation pulses were formed by frequency doubling the output of a light conversion TOPAS-C optical parametric amplifier to yield laser pulses from 3.85 eV to 3.97 eV with an intensity of approximately 5-10 μJ/pulse at the vacuum chamber. The remaining fundamental was used as the probe with an intensity of approximately 85 μJ/pulse. The cross correlation of the pump and probe pulses was less than 150 fs. One-color spectra were obtained by blocking the fundamental and only using the UV light. For these experiments, photon energies of 4.28 eV-4.97 eV were used with intensities ranging from 3 to 9 μJ/pulse. Photoelectrons resulting from the interaction between the laser and the anion clusters were accelerated using velocity map imaging (VMI) towards a position sensitive detector. These VMI images were processed using the basis-set expansion (BASEX) reconstruction method[63] for electron kinetic energy distributions and polar onion peeling[64] (POP) for photoelectron angular distributions (PADs).

B. Computational

All electronic structure calculations were performed using the Gaussian 09 program package.[65] Minimum energy geometries of bare A9, A7, and A3 and the corresponding neutral and anionic I·A complexes were optimized using Møller Plesset perturbation theory (MP2) combined with an augmented Dunning basis set for adenine (AUG-cc-pVDZ) and an expanded basis set with an increased set of diffuse functions for iodide.[66] Frequency calculations verified that the optimized geometries represent minimum energy structures (no imaginary frequencies). VDEs were calculated as the energy difference between the neutral and the anionic clusters at the equilibrium geometry of the anion using coupled cluster singles and doubles (CCSD) with the same basis set as was used for the MP2 geometry optimizations. Similarly, the cluster AEAs were calculated as the energy difference between the optimized neutral and the optimized anion of the clusters. MP2 based zero-point energy (zpe) corrections were also evaluated. Cluster dipole moments were extracted from the CCSD single point calculations on the geometries optimized at the MP2 level of theory. The dipole moments of specific interest are those associated with the vertical and relaxed cluster geometries of the $(I{\cdot}DB)^-$ states. These were taken to be the dipole moments of the neutral complex at the geometry of the anionic ground states and the neutral equilibrium state, respectively.

In order to understand the energetics and the transformation between DB and VB anions of A9, A7, and A3 tautomers, we performed long-range corrected density-functional theory (LC-DFT) calculations that can describe both DB and VB anions and their interconversion. Several LC-DFT functionals are available in recent quantum chemistry codes, and we have chosen to employ the CAM-B3LYP method combined with the standard 6-311++G(2d,p) basis set augmented with five sets of diffuse *sp* functions on hydrogen atoms (with an exponential scaling factor $\alpha = 2$). The geometries of gas phase neutral A9, A7, and A3 were optimized, and from these calculations, the DB and VB anion geometries, the VDEs of the DB and VB anions of bare A9, A7, and A3, and the corresponding AEAs were calculated. It is important to stress that the estimated VDEs and AEAs (especially the negative ones) should be interpreted cautiously. The properties of π^* VB anions are difficult to investigate theoretically,[67] particularly when the anion is higher in energy than the corresponding neutral. In such cases, the VB anion corresponds to a quantum mechanical continuum state, and the computational results will be very sensitive to the treatment of correlation interactions and the inclusion of extra diffuse functions in the basis set. In the current investigation, the A9 tautomer represents an especially challenging system as elaborated below.

DB ↔ VB interconversion was traced with a linear scaling scheme, where geometries between DB and VB structures were linearly interpolated. The linear scaling scheme is equivalent to what we employed previously[68] and to work by the Sommerfeld group.[38] Here, the geometries between the DB and VB anions are defined as $X(s) = X_{AnDB} - s \cdot (X_{AnDB} - X_{AnVB})$, where s is a dimensionless reaction coordinate parameter taking values from 0 to 1, X_{AnDB} represents the equilibrium DB anion ($s = 0$), and X_{AnVB} is the equilibrium VB anion ($s = 1$) of the respective adenine tautomers (n, where n denotes 9, 7, and 3). In the case of A9, the procedure was slightly different due to the computational difficulties of evaluating the properties of the A9 VB anion as mentioned above. We found that a stable A9 VB anion structure cannot be located on the potential energy surface obtained from the LC-DFT calculations with diffuse basis functions, due to the significant influence from the A9 DB state. Similar difficulties of optimizing an A9 VB anion minimum have been reported previously both using DFT and *ab initio* methods, see for instance Ref. 52. Therefore, the A9 VB structure at $s = 1$ was optimized using LC-DFT without diffuse basis functions, and the results should be interpreted within this limitation. Furthermore, the VDE of the A9 VB anion and the corresponding AEA were estimated from the energies associated with the geometry at $s = 1$, though this does not correspond to a true minimum. We also investigated tautomerization and anion transformation from A9 DB to A3 VB. In this case, the linear scaling scheme can be defined as

$$X(s) = X_{A9DB} - s \cdot (X_{A9DB} - X_{A3VB}).$$

III. RESULTS AND ANALYSIS

A. Calculated structures and energies of adenine-iodide complexes

The gas phase energies of optimized A7 and A3 were calculated at the MP2/aug-CC-pVDZ level to be, respectively, +0.31 eV and +0.33 eV relative to the canonical A9 tautomer, both matching the values reported in the literature[49,69] and the CAM-B3LYP/6-311++G(2d,p) energies calculated here. The lowest energy conformers of the neutral and anion I·A9 and I·A3 clusters are shown in Figure 1 including key structural parameters. As discussed in Sec. IV A, no indications of I$^-$·A7 are observed in the experiment, so the I$^-$·A7 cluster is not shown in Figure 1. Upon iodide complexation, the A3 tautomer is stabilized by 0.13 eV relative to A9, which reduces the energy difference to 0.2 eV.

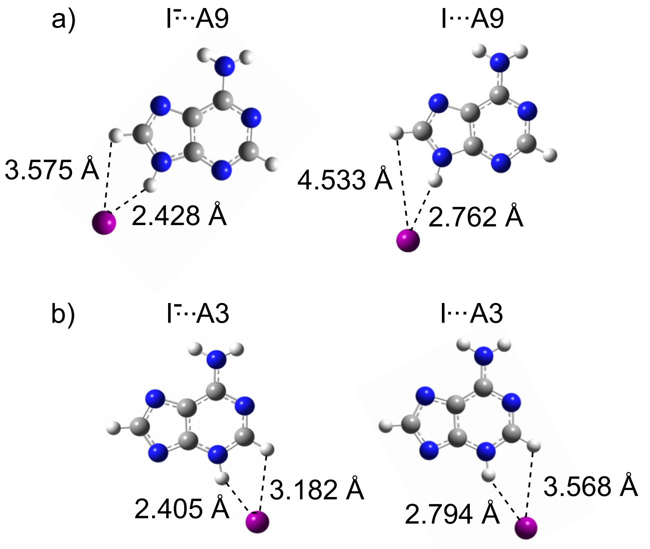

FIG. 1. Optimized geometries including central structural parameters of (a) I·A9 and (b) I·A3 neutral and anionic complexes.

Table I summarizes calculated energetics and dipole moments for anionic and neutral complexes. At the CCSD/aug-CC-pVDZ level of theory, calculated VDEs of the I$^-$·A clusters for A9, A7, and A3 are 4.01 eV, 4.5 eV, and 4.15 eV, respectively, and the AEAs of the neutral complexes are 3.93 eV, 4.19 eV, and 3.98 eV (including MP2 zpe corrections). The cluster dipole moments of neutral I·adenine in the Franck-Condon (FC) and relaxed geometries (Figure 1) were found to be 4 D and 3.1 D, respectively, for I·A9 and 5.6 D and 5.1 D for I·A3. The structures of A9 DB, A3 DB, and A3 VB are shown in Figure 2; the structure of A9 VB is omitted since no minimum was located. DB anions for the three gas phase bases have positive VDEs ≈ AEAs in the range 0.02-0.265 eV. Due to the structural similarity between the DB anion and the corresponding neutral, the VDEs and the AEAs are approximately the same. Adiabatic binding energies are negative for the VB anions of A9 and A7 and positive by 120 meV for A3, consistent with the literature.[49] The theoretically estimated VB anion VDEs are >0.5 eV for A7 and A3. For A9, the VDE at $s = 1$ was found to be 0.135 eV, but this value has little physical meaning as the structure does not correspond to an actual minimum on the potential energy landscape. Thus, while the calculations point towards an adiabatically and possibly vertically unbound A9 VB anion, the results should not be interpreted in a quantitative matter.

In order to understand the DB ↔ VB anion transformation processes for bare A9, A3, and A7 tautomers, we calculated

TABLE I. Calculated energies and dipole moments of A9, A3, and A7 in the gas phase and in anionic clusters. The level of theory is indicated in the parentheses. For the CCSD calculations, the basis set was AUG-cc-pVDZ further augmented on iodide, and for the CAM-B3LYP calculations, the basis set was 6-311++G(2d,p) augmented on hydrogen as described in Sec. II B and 6-311+G(2d,p) for the VB VDE calculations. The experimentally measured VDEs are included for comparison.

	A9	A3	A7
I$^-$·A VDE (CCSD) (eV)	4.01	4.15	4.5
I$^-$·A VDE (experimental)	3.96 eV	4.11	…
I·A AEA (CCSD)[a] (eV)	3.93	3.98	4.19
μ (I·A Franck-Condon geometry) (D)	4	5.6	
μ (I·A relaxed geometry) (D)	3.1	5.1	5.1
μ (A gas phase) (D)	2.5	4.7	6.8
Bare DB VDE ≈ AEA (CAM-B3LYP) (eV)	0.02	0.057	0.265
Adiabatic eBE of bare VB anion (CAM-B3LYP) (eV)	−0.497[b]	0.120	−0.201
Bare VB VDE (CAM-B3LYP) (eV)	0.135[b]	0.686	0.501

[a] Zero-point energy corrected with MP2/AUG-cc-p VDZ zero-point energies.

[b] The values refer to the s = 1 point on the potential energy surface and does not correspond to a true minimum.

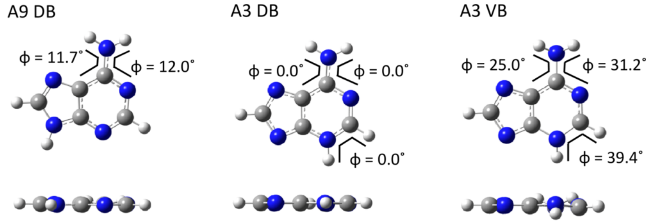

FIG. 2. Geometries of A9 DB, A3 DB, and A3 VB.

potential energies for neutral and anionic states along linearly scaled geometries at the CAM-B3LYP level as described previously. All energies presented in Figure 3 are referenced to the energy level of the most stable A9 DB anion. Figure 3(a) displays the potential energy profiles for A9. As mentioned previously, the $s = 1$ A9 VB structure was optimized without diffuse basis functions to obtain a non-planar π* VB anion structure. It is worth mentioning that the obtained structure is very similar to the VB anion structure of Raczyńska *et al.*[49] which was optimized at the B3LYP/6-311+G(d,p) level. The calculated anion potential energy monotonically increases from $s = 0$ to 1 and no minimum is observed. However, we found that the binding mechanism of the excess electron smoothly changes from the DB towards a VB anion, and that the VDE value is slightly increased. In Figure 3(a), we also show the tentative potential energy (shaded region) for the metastable π* VB anion state within a local-complex theory picture.[70] Since this state is embedded in the electron scattering continuum, the corresponding potential energy has energetic uncertainty depending on the electron autodetachment lifetime. It should be emphasized that the metastable π* A9 VB anion, corresponding to a scattering state, cannot totally be described by the present DFT method using a set of Gaussian basis functions. The potential energy curve with energy widths is therefore shown to approximately reproduce the previous electron transmission spectroscopy experiments,[1,50] which suggest that the π* VB state is +(0.45-0.54) eV higher in energy above the neutral A9 minimum energy structure. We note that quantum electron scattering calculations have also been carried out at the A9 minimum structure.[71–73] According to these studies, the lowest metastable π* resonance state is calculated to be in the energy range of 1.1–2.4 eV above the A9 minimum, which is somewhat larger than the above-mentioned electron transmission spectroscopy result.

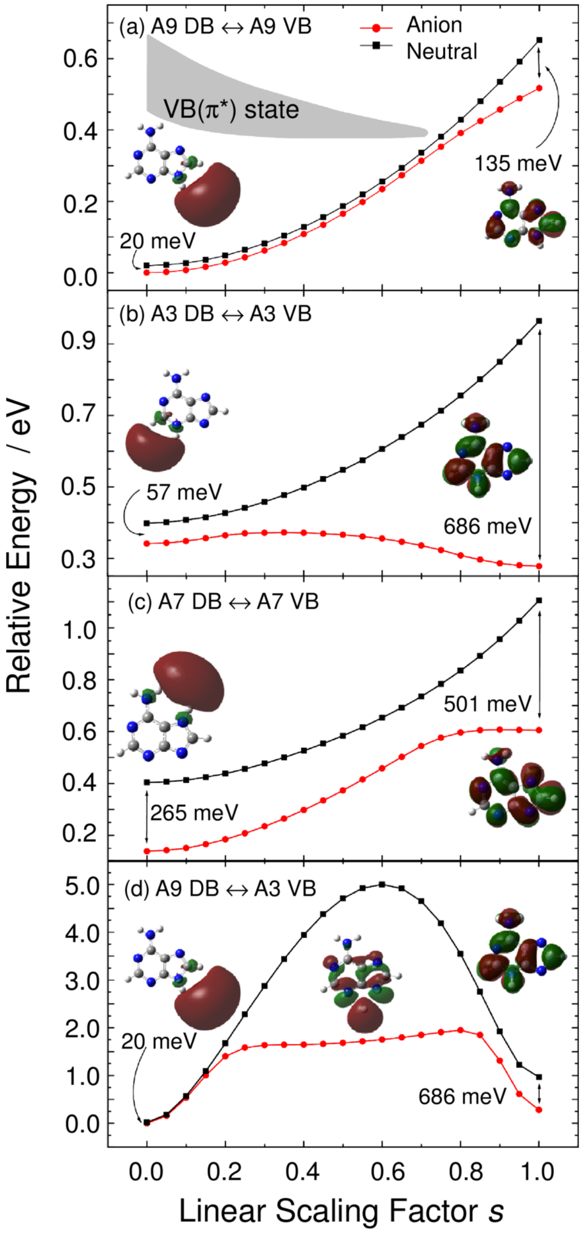

FIG. 3. Potential energy surfaces associated with DB to VB transition for (a) A9, (b) A3, (c) A7, and (d) A9 DB to A3 VB, calculated using CAM-B3LYP/6-311++G(2d,p) augmented with five sets of diffuse *sp* functions on the hydrogen atoms with an exponential scaling factor $s = 2$. In all cases, the energy scale is adjusted relative to the most stable species; the dipole bound anion of the canonical A9 tautomer.

Figure 3(b) shows the energy profile between the A3 DB and A3 VB structures. The A3 VB anion has a non-planar structure and is more stable than the A3 DB anion by 65 meV (1.5 kcal/mol). There is a very small barrier of 30 meV (0.7 kcal/mol) on the pathway from A3 DB to A3 VB, but this is not a true transition state. However, this calculation indicates that the A3 DB anion can easily convert into the A3 VB anion, though the effect of iodide is not taken into account. Figure 3(c) shows potential energy profiles similar to Figure 3(b), but for the A7 tautomer. In this case, the A7 DB anion has a large VDE (265 meV) due to the large dipole moment of the neutral core (6.8 D[44]), but the A7 DB → A7 VB process is found to be endothermic and associated with a barrier of 550 meV (12.68 kcal/mol). This VDE for the A7 DB state is somewhat larger than the previous theoretical results.[49]

Figure 3(d) shows the potential energy profiles from A9 DB to A3 VB along the linear scaling coordinate s. The anionic potential energy profile from A9 DB to A3 VB shows characteristics of two avoided crossings at $s \sim 0.2$ and 0.8. The former point corresponds to the change of the excess electron occupation from the DB to the σ* orbital, and the latter to population transfer from the σ* to the π* orbital. This figure implies that the A9 DB anion cannot easily isomerize into the A3 VB anion due to the very high barrier of 1.7-2.2 eV (40-50 kcal/mol).

B. One-color spectra

One-photon photoelectron spectra of the $I^-{\cdot}A$ clusters recorded at photon energies hν from 4.28 to 4.97 eV are shown in Figure 4 with the normalized intensity plotted as a function of electron binding energy defined by eBE = hν − eKE, where eKE is the electron kinetic energy. The spectra show three features: feature A with a constant eBE of 3.96 eV and a shoulder, A′, at 4.11 eV, feature B with a varying eBE but constant eKE of approximately 0.25 eV, and feature C at eBE = 4.90 eV. Feature B is only present in the spectra recorded at photon energies 4.69-4.97 eV and is slightly obscured at 4.97 eV due to feature C, which grows in with eBE = 4.90 eV at the highest photon energy. The anisotropy parameters, β_2, associated with the spectral features were obtained by fitting the PADs to the following equation:[74]

$$I(\theta) = \frac{\sigma_{total}}{4\pi}\left[1 + \beta_2 P_2(\cos\theta)\right], \qquad (2)$$

where σ_{total} denotes the total photodetachment cross section, θ represents the angle between the laser polarization and the detached electron, and P_2 is the second Legendre polynomial. Values of β_2 range from −1 to 2 corresponding to perpendicular and parallel detachment, respectively. The anisotropy parameters associated with features A and B are approximately −0.5 and +(0-0.5), respectively. Feature C is only present at 4.97 eV, where it overlaps with feature B. At this photon energy, B and C fall in the near-zero eKE region (near the maximum eBE), where the POP reconstruction method is less accurate due to center-point noise obscuring the photoelectron signal,[30,64] and the anisotropy value for feature C (and B at this photon energy) is therefore less reliable.

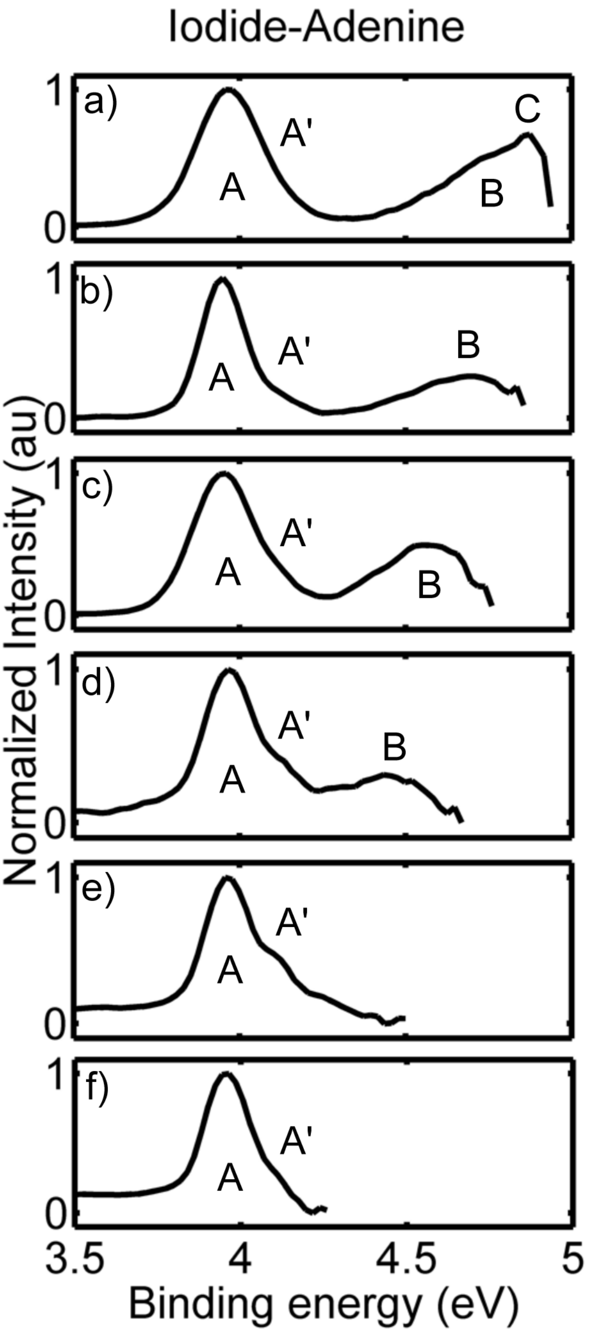

FIG. 4. One-color spectra of $I^-{\cdot}A$ clusters using photon energies: (a) 4.97 eV, (b) 4.88 eV, (c) 4.78 eV, (d) 4.69 eV, (e) 4.52 eV, and (f) 4.28 eV.

The eBE-invariant feature A at eBE = 3.96 eV corresponds to vertical detachment from the $I^-{\cdot}A9$ complex, and feature C, which appears 0.94 eV higher in energy relative to feature A, corresponds to detachment to the upper iodine spin-orbit state ($^2P_{1/2}$) from the $I^-{\cdot}A9$ complex. Feature B with the photon-invariant eKE is only present at some excitation energies, all overlapping with the UV gas phase absorption of the A9 tautomer.[56] Neither the analog to feature B nor the shoulder in the main cluster detachment peak (feature A′) was observed in one-photon PE spectra of $I^-{\cdot}$uracil and $I^-{\cdot}$thymine.[27,28]

C. Time-resolved photoelectron spectroscopy

Time-resolved PEI experiments were performed at four different pump energies in the range 3.85-3.97 eV corresponding to −110 meV, −60 meV, −20 meV, and +10 meV relative to the VDE of $I^-{\cdot}A9$ (3.96 eV), and thereby at significantly lower energies than the energy region explored in the one-photon experiments. Time-resolved signal at excitation energies higher than 3.97 eV was much less distinct. Contour plots extracted from the time-resolved experiments showing eBE (=$h\nu_{probe}$− eKE) vs. pump-probe time delay are shown in Figures 5(a)-5(d). These plots show two main features: feature *I* is narrow and appears within a few hundreds of fs at eBE = 0-0.2 eV, and feature *II* grows in after a few ps as a broader peak spanning eBE = 0.2-0.8 eV. Feature *II* is artificially broadened by a third component (feature *III*) at 0.79 eV, present at both negative and positive times, resulting from direct detachment of the ground state complex by three probe photons. Similarly, direct detachment of the ground state complex by the pump and the probe pulse results in feature *IV*, a narrow peak at time-zero that contaminates feature *I* slightly at 3.85 eV. Based on the previous investigations,[75] features *I* and *II* can be identified as probe-induced detachment from, respectively, DB and VB anions of the $(I{\cdot}\text{adenine})^-$ complexes.[27–31] Even by visual inspection, it is apparent that feature *I* is both longer-lived and considerably more prominent relative to feature *II* at 3.94 eV.

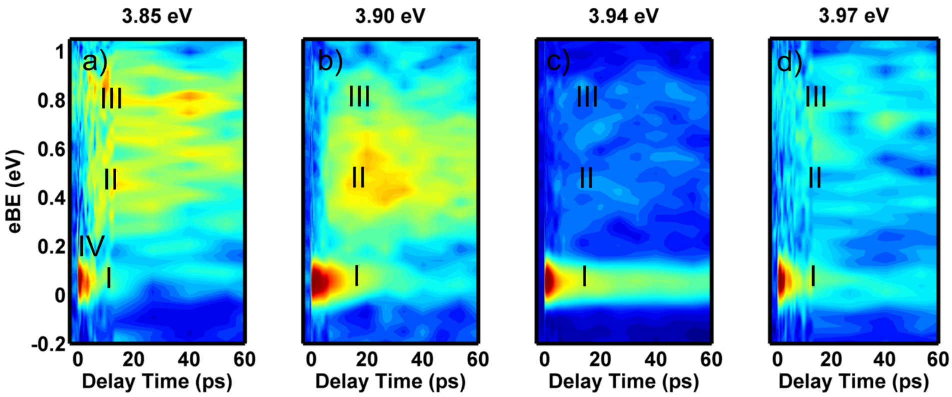

FIG. 5. Contour plots of I$^-$·A clusters from the TRPEI experiments at pump energies: (a) 3.85 eV, (b) 3.90 eV, (c) 3.94 eV, and (d) 3.97 eV. In all cases, 1.58 eV was used as probe energy. Features *I–IV* correspond to the dipole bound anion, valence bound anion, three probe photon detachment of the ground state complex, and pump and probe photon detachment of the ground state, respectively.

In order to quantify the intensity changes of features *I* and *II*, the spectra were analyzed by channel-integrated fitting and global fitting. The channel-integrated and normalized intensities are plotted as a function of time delay in Figures 6(a)-6(d). These transients were fitted to a sum of exponentials convoluted with a Gaussian instrument response function (IRF),

$$I(t) = \frac{1}{\sigma_{cc}\sqrt{2\pi}} \exp\left(-\frac{t^2}{2\sigma_{cc}^2}\right) * \begin{cases} I_0, t < 0 \\ I_0 + \sum_i A_i \exp\left(-\frac{t}{\tau_i}\right), t \geq 0 \end{cases}. \tag{3}$$

The fits are shown in Figures 6(a)–6(d) and the associated lifetimes are summarized in Table II. Feature *I* can be fit to a constant mono-exponential rise of 250 fs (within error bars) at all excitation energies except 3.85 eV. At 3.85 eV, feature *IV* overlaps on the eKE scale with feature *I* and dominates the spectrum at time-zero, which obscures the lane integrated fits of the DB rise time. Feature *IV* is present at all four excitation energies, but it only has significant amplitude at 3.85 eV. The decay of feature *I* fits a single exponential at 3.85 eV and 3.90 eV, but requires two exponentials at 3.94 eV and 3.97 eV. The initial decay ranges from 3 to 11 ps and is fastest at highest excitation energies. The slower decay is approximately 1 ns at 3.94 eV and a few hundreds of ps at 3.97 eV. Feature *II* can be fit to a mono-exponential rise of 4-10 ps and a constant mono-exponential decay of ≈70 ps. At all four excitation energies, the rise time of feature *II* matches the faster (or only) decay of feature *I* within error bars.

Table II also includes the ratios of the components related to each exponential. For feature *I*, the ratio of the fast decay versus the rise ($A_{\tau_{decay\ 1}}/A_{\tau_{rise}}$) is fairly constant, while the

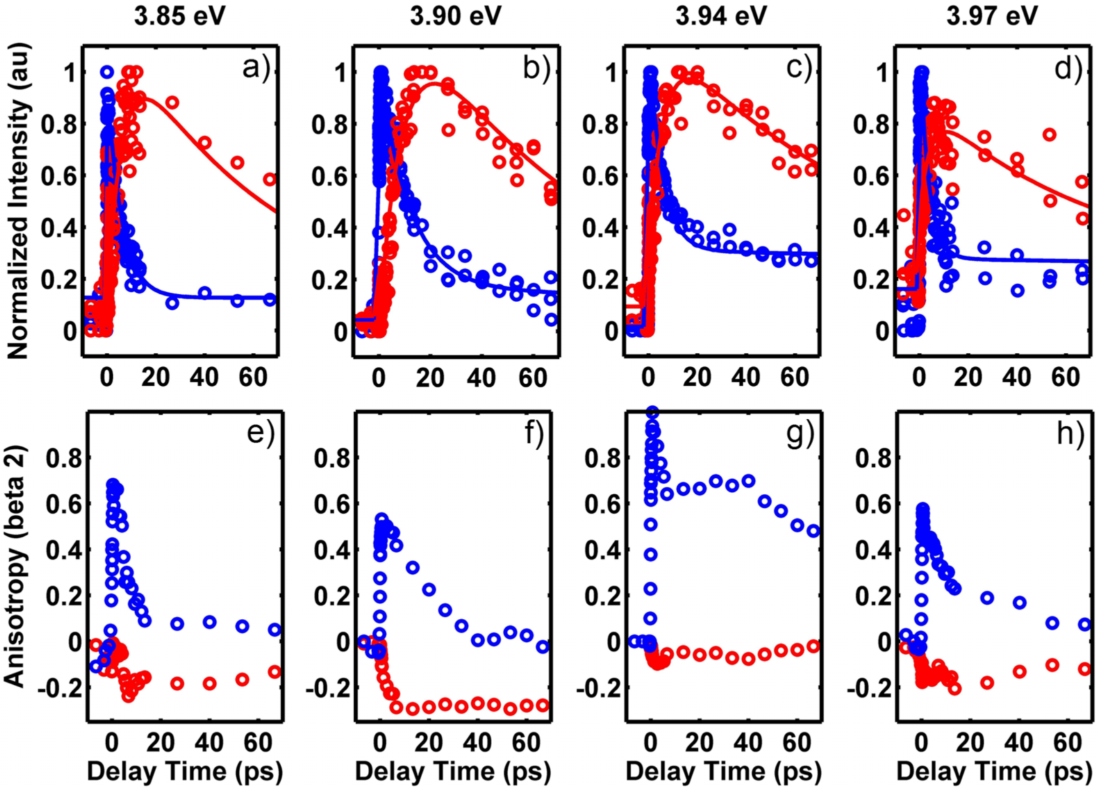

FIG. 6. Temporal evolution of the normalized intensities ((a)-(d)) and β_2-values ((e)-(h)) of feature *I* (DB state, blue) and feature II (VB state, red) at excitation energies (a) and (e) 3.85 eV, (b) and (f) 3.90 eV, (c) and (g) 3.94 eV, and (d) and (h) 3.97 eV.

TABLE II. Lane integrated fits and ratios.

Dipole bound anion

Excitation energy (eV)	Rise (fs)	Decay 1 (ps)	Decay 2	$\frac{A_{\tau_{decay\,1}}}{A_{\tau_{rise}}}$	$\frac{A_{\tau_{decay\,1}}}{A_{decay\,2}}$
3.85	100-250[a]	6-7.50		1.7	…
3.90	230 ± 38	11.0 ± 0.8		1.5	…
3.94	297 ± 35	4.8 ± 0.3	1.07 ± 0.18 ns	1.05	2.5
3.97	245 ± 61	2.7 ± 0.4	152 ± 59 ps	1.1	3.8

Valence bound anion

Excitation energy (eV)	Rise (ps)	Decay 1 (ps)	$\frac{A_{\tau_{decay\,1}}}{A_{\tau_{rise}}}$	DB/VB
3.85	6 ± 0.7	64 ± 6	1.01	≈1
3.90	10.1 ± 1	62.1 ± 6.6	1.01	≈1
3.94	5.8 ± 0.6	99.7 ± 5.8	1.2	>3
3.97	4.3 ± 1	71.3 ± 10.2	1.5	≈1

[a] Obscured by three photon component.

branching of the two decays ($A_{\tau_{decay\,1}}/A_{\tau_{decay\,2}}$) shows that the slow decay ($\tau_{decay\,2}$) is more prominent at 3.94 eV than at 3.97 eV. The intensity ratio of features *I* and *II* varies with excitation energy and time delay. When estimated at the time delay where the normalized transients in Figure 6 cross, the integrated intensity ratio (DB/VB in Table II) is approximately 1 at 3.85 eV, 3.90 eV, and 3.97 eV and approximately 3 at 3.94 eV. However, since the long decay component is much more prominent at 3.94 eV, the value of DB/VB = 3 is an underestimate of the DB contribution to the total electron flux at 3.94 eV. Regardless, the DB feature is much more prominent at 3.94 eV than at any of the other excitation energies.

The anisotropy parameters for time-resolved PEI data were again obtained by fitting the PADs to Eq. (2).[74] The temporal evolutions of β_2 at all excitation energies are shown in Figures 6(e)-6(h). At excitation energies other than 3.94 eV, β_2 for feature *I* increases from 0.0 to 0.5-0.6 at time-zero and decays to zero as the signal decays. At 3.94 eV, the value of β_2 for feature *I* reaches 1.0 at zero time delay. It then decays to approximately 0.6 at about 7 ps and remains relatively constant to about 50 ps, after which it drops somewhat. At all four excitation energies, values of β_2 for feature *II* range from 0 to −0.3 at the time delays where feature *II* shows signal intensity.

When possible, a global fitting procedure was applied. In global fitting, the entire spectrum is fit simultaneously in energy and time with shared parameters according to the following equation:[76,77]

$$S(eKE,t) = \sum_i k_i\,(eKE)\left[\exp\left(-\frac{t}{\tau_i}\right) * g(t)\right], \qquad (4)$$

where $k_i\,(eKE)$ is the decay-associated spectrum (DAS), shown in Figures 7(a)-7(c), associated with the *i*th spectral feature decaying exponentially with a lifetime of τ_i, and the Gaussian IRF is accounted for by $g(t)$. Global fitting is powerful for fitting spectral response of population transfer since the fitting does not depend on how the integration regimes are selected. However, the algorithm can only fit data for which each state has a static spectrum; if the eKE shifts over time or if there are large-amplitude motions, the algorithm is not applicable. The global fitting procedure was unsuccessful for the data recorded at 3.94 eV, possibly due to the slight peak shifting of feature *I* and the substantial intensity difference between features *I* and *II* resulting in poor treatment of feature *II*.

Figure 7 shows the DAS, the contour plots of the raw and the fitted data, and the associated residuals. When applied, the global fitting analysis requires three (or four at 3.97 eV) components resembling a rise and a mono- or bi-exponential decay in the spectral region of feature *I* and a rise and mono-exponential decay in the spectral region of feature *II* as shown in the DAS. In the DAS, the negative components illustrate a rise in that specific spectral region, and the positive components correspond to decays. Population flow from one state to another therefore shows up as a concomitant (same colored curve in the DAS) change in the positive and negative components of the particular energy areas in the spectrum; this is most evident in the green curves in Figs. 7(a) and 7(b). At 3.85-3.90 eV, a clear DB to VB population transfer is observed. It is also seen, but less clearly, at 3.97 eV. The fitted lifetimes, shown in Table III, agree well with the fits obtained from lane-integrated fitting. At 3.85 eV, feature *IV* obscures feature *I* at time-zero. This was accounted for by adding an extra component of 10 fs capturing the two-photon process, while only minimally disturbing the fit of feature *I*. This extra component is left out in the DAS for clarity, as it has no relevance for the anion dynamics.

IV. DISCUSSION

A. One-color spectra of I^-·adenine anionic clusters

The one-color spectra of I^-·adenine clusters, Figures 4(a)-4(f), show a different number of peaks depending on the photon energy. In all cases, the dominant feature (A) appears at eBE = 3.96 eV. This value is the VDE of I^-·A9 and is in reasonable agreement with the CCSD calculated value of 4.01 eV—a slight overestimation of the calculated VDE relative to the experimental value is consistent with our previous results on iodide complexes.[27–31] The anisotropy parameter, −0.5, is consistent with photodetachment from an iodide complex where the charge density primarily is localized on iodide,[78] as expected for the ground state I^-·adenine complex. The two most likely origins of the shoulder A′ at 4.11 eV are FC active modes in the I^-·A9 complex or, in light of previous investigations of adenine,[47,48,79,80] detachment from an I^-·adenine complex comprising a different adenine tautomer. Considering the structural similarities (Figure 1) between the anionic complex and the corresponding neutral, it appears unlikely that the shoulder originates from FC activity. The main (but small) structural differences include distances and angles involving iodide and adenine, all modes that are considerably lower in energy (0.01-0.02 eV) than the observed 0.15 eV spacing and unlikely to be resolved by our femtosecond laser pulses (0.040 eV bandwidth). Furthermore, similar features were not observed in I^-·uracil or I^-·thymine complexes where the geometrical differences were similar or

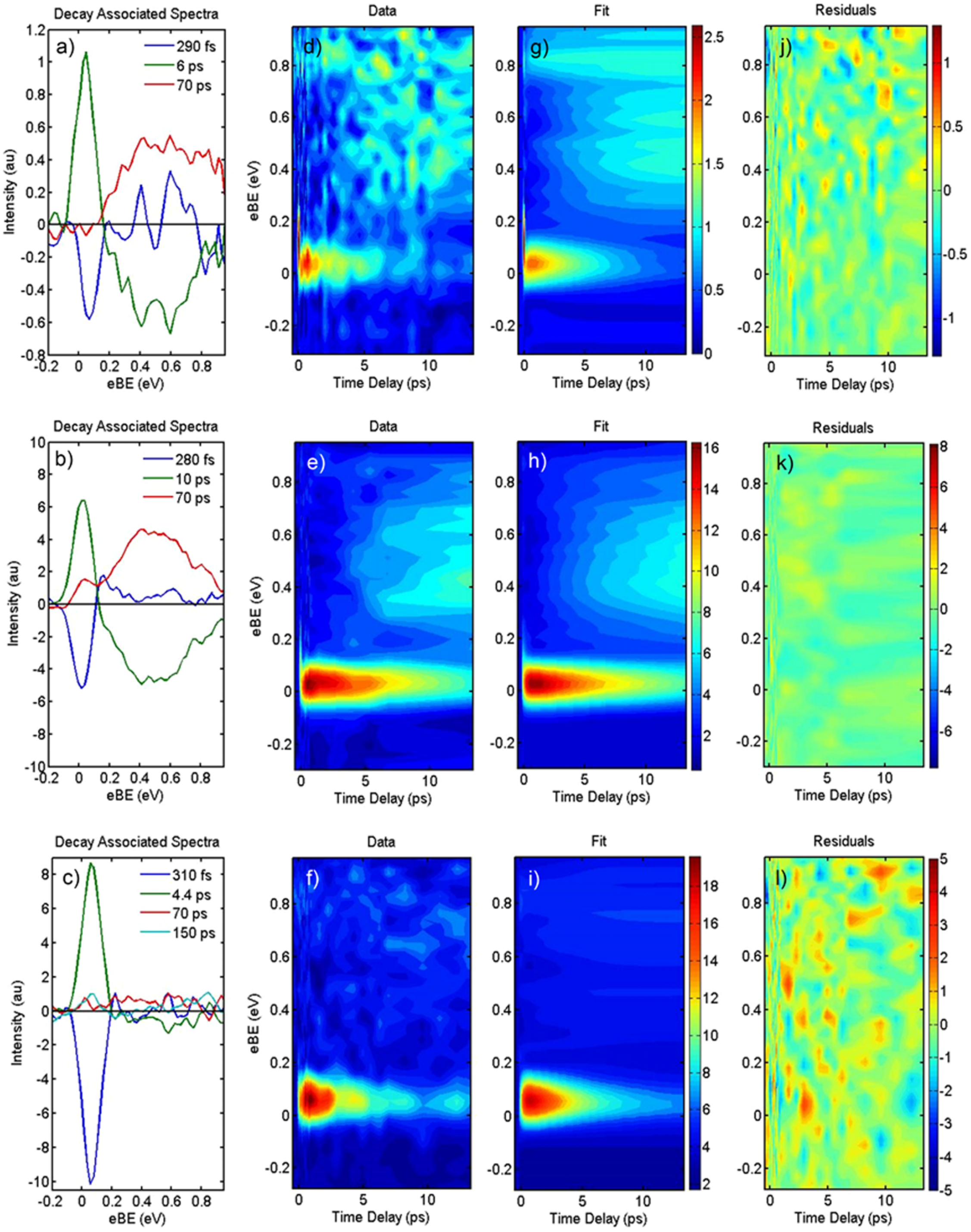

FIG. 7. Decay Associated Spectra (DAS) ((a)-(c)), contour plots of the raw data ((d)-(f)), the fitted data ((g)-(i)), and the residuals ((j)-(l)) at 3.85 eV, 3.90 eV, and 3.97 eV (top to bottom).

even slightly larger.[31] It thus appears that the shoulder observed for adenine is not due to FC activity, and we therefore consider the presence of other tautomers.

The most abundant tautomers are A9, A7, and A3 (Scheme 1),[49] all of which are represented by an amine form and differ according to the location of the heterocyclic N–H bond. While A7 and A3 are less thermodynamically favored than A9 (by 0.31 eV and 0.33 eV, respectively), they could be formed in the ion source due to the need for heating the sample to obtain sufficient adenine concentration in the vapor phase, potentially causing some degree of tautomerization. The eBE of the shoulder A′ matches the CCSD calculated VDE of $I^-{\cdot}A3$ of 4.15 eV. In contrast, we estimate a VDE of $I^-{\cdot}A7$ of 4.50 eV where no distinct detachment feature is observed. The occurrence of $I^-{\cdot}A3$ will be considered further when discussing the time-resolved PEI results.

B. One-color spectra: Shape resonances

At photon energies from 4.69 to 4.97 eV, feature B grows in and distinguishes itself by exhibiting a varying eBE, but a constant eKE of about 0.25 eV. This trend implies that feature B does not originate from vertical detachment, but rather from a different type of process. Moreover, the value of β_2 for feature B is observed to be between 0 and 0.5 at all photon energies, higher than the negative value expected from an electron originating from an iodide complex.[78] Interestingly, feature B grows in as the photon energy enters the UV absorption band of A9 and is most prominent at the maximum UV absorption.[56,81] Previous investigations from our laboratory on clusters with uracil and thymine also included photon energies in the absorption band of the respective nucleobases, but similar peaks were not observed in those cases.[27–31]

We hypothesize that feature B corresponds to (π,π*) absorption of A9 followed by rapid electron transfer from iodide into the empty π orbital according to the following equation:

$$I^- \cdots A9\,(ground\ state) \xrightarrow{hv} I^- \cdots A9\,(\pi,\pi^*) \xrightarrow{electron\ transfer} I \cdots A9^-_{VB} \rightarrow I \cdots A9 + e^-\,(eKE \approx 0.25\ \text{eV})\,. \tag{5}$$

This mechanism essentially corresponds to formation of a VB A9 anion with a geometry resembling the FC geometry (corresponding to the shaded region in Figure 3(a)). The VB A9 anion is both experimentally[1,50,51] and theoretically[52] predicted to be unbound, and the electron should therefore auto-detach efficiently and appear in the spectra as a shape resonance. The constant eKE of the detached electron suggests that as the photon energy is varied across the band, the additional vibrational energy in the π* state is conserved upon autodetachment rather than channeled into electron kinetic energy.

This interpretation rests on the assumption that electron transfer from iodide to electronically excited A9 competes efficiently with internal conversion (IC) in A9, which has been measured to occur on a time scale of approximately 1 ps at similar excitation energies in the gas phase.[82] Considering the proximity between iodide and adenine in the complex (Figure 1(a)), it is plausible that electron transfer is rapid and capable of competing with IC. In the case of uracil and thymine, evidence of the corresponding process was not observed,[27] most likely because the VB anions in those cases are bound; while UV absorption possibly occurs as well, it should not give rise to a similar signal in the photoelectron spectra. This indirect observation adds to the existing hypothesis that the VB anion is unbound (although it does not conclusively prove it), and the following discussion on the time-resolved PEI results will therefore follow this premise.

C. Time-resolved experiments

Upon excitation of I^-·adenine complexes near the VDE, the electron can either detach from the system with low eKE, leaving a neutral complex behind, or transfer to adenine in a (largely) vertical process. The latter results in a negative ion with the character of either a dipole or a valence anion.[27–31] At all excitation energies studied here, a sharp peak at low eBE, feature *I*, and a broad peak at higher eBE, feature *II*, are observed. These peaks exhibit the spectral characteristics of DB and VB anions, respectively,[29–31,75] and will be referred to accordingly from here on. The key observations to be covered in this section include a constant DB anion rise time of 250 fs (feature *I*), consistent with previous observations in I^-·uracil and I^-·thymine, and an apparent DB to VB anion transition that at first glance appears similar to the transition observed in nitromethane,[30] but different from that observed for I^-·uracil and I^-·thymine.[29,31] We also see features that distinguish the adenine data from the systems previously examined in our group. These differences include the observation of a VB feature with a VDE larger than that expected for the canonical A9 VB anion, the DB anion intensity and the DB/VB anion intensity ratio showing non-monotonic trends with excitation energy, and the DB anion decay dynamics being mono-exponential at some excitation energies and bi-exponential at others.

TABLE III. Lifetimes obtained from global fitting.

Excitation energy (eV)	Lifetimes of components in decay associated spectra			
3.85	290 fs	6 ps	(70 ps)	…
3.90	280 fs	10 ps	70 ps	…
3.94	…	…	…	…
3.97	310 fs	4.4 ps	70 ps	150 ps

1. *Initial dynamics of the dipole- and valence bound anions*

The DB anion represented by feature *I* exhibits a constant rise time of about 250 fs at all excitation energies, similar to the rise time seen in our previous experiments on I^-·uracil and I^-·thymine.[29,31] For the DB states in I^-·uracil and I^-·thymine, we found that the potential energy surfaces are repulsive in the FC region along the iodine-base coordinate, causing the iodine atom to move away from the nucleobase. As discussed at length in previous work, these dynamics affect the diffuse orbital in which the DB electron resides, resulting in an increased photodetachment cross section that manifests itself as a non-zero rise time for feature *I*.[31] The geometrical differences between the anionic ground state and the neutral I·adenine complexes (Figure 1) also mainly involve the parameters related to the binary binding motifs, and the potential energy landscape of the DB anion in the FC region for the I·adenine complex is expected to be similar to those of

I·uracil and I·thymine. The observation of a non-zero rise time for feature *I* is therefore ascribed to iodine-adenine motion and an accompanying increase in the photodetachment cross section from the DB anion.

At all excitation energies, the DB anion shows a fast decay component ranging from 3 to 11 ps, which is mirrored by a simultaneous rise of the VB state, feature *II*. Equivalently, the green curve in the DAS (Figures 7(a)-7(c)), corresponding to the dynamics associated with a 4-10 ps lifetime, shows positive amplitude in the DB spectral region and negative amplitude in the VB region and thus implies population flow from the DB into the VB state. We therefore ascribe the fast decay component of the DB feature to the DB to VB anion transition. These dynamics are particularly prominent at 3.85 eV and 3.90 eV and slightly less significant at 3.97 eV due to smaller amplitude of the VB anion signal intensity relative to the DB anion, which is discussed further in Sec. IV C 3. To this end, the DB to VB anion transition appears similar to previous observations for nitromethane;[30] such a transition was expected for nitromethane where the VB anion is well-known to be the anionic ground state.[83–85] In contrast, as discussed in Sec. III A, the VB anion of at least the canonical A9 tautomer of adenine is expected to be higher in energy than the DB anion and unstable with respect to the neutral.

2. Origin of a bound valence anion of adenine

The observed detachment energy of the VB feature spans the energy range of approximately 0.25-0.8 eV, suggesting that the observed VB anion should not be ascribed to the A9 VB anion, which is estimated to have a near zero detachment energy, cf. the reported VDE of +0.03 eV (B3LYP/6-311+G(d,p))[49] and the calculated VDE at $s = 1$ (though this is not a true minimum) of +0.135 eV (CAM-B3LYP/6-311G(2d,p)) in this work. We must therefore consider alternative explanations for the observation of the VB feature. Of the most abundant tautomers, both A7 and A3 support VB anions with VDEs matching the experimental results (+0.501 eV and +0.686 eV, respectively), but only A3 is predicted to have an adiabatically bound VB anion (Table I). We explored the potential energy surfaces associated with DB to VB anion transition for all three tautomers, as shown in Figure 3. When the pump pulse interacts with the complex and induces electron transfer, some vibrational excitation accompanies the DB anion formation. In our previous investigation on uracil and thymine, the initial vibrational excitation was found to primarily be localized in the low-frequency I-base libration modes,[29,31] and similar localization of the initial vibrational excitation in adenine is assumed here, consistent with the observation of a sharp peak for the DB feature in the photoelectron spectra. Hence, the nucleobase in the initially formed DB state should have relatively little vibrational excitation.

As can be seen in Figure 3, the DB to VB transition is energetically unfavorable for both A9 and A7 and associated with barriers >0.45 eV, i.e., well above the energy expected to be deposited as vibrational energy in the base itself upon excitation and initial intramolecular vibrational energy redistribution. The lack of a VB anion minimum for A9 suggests that A9 autodetaches long before any A9 VB anion formation occurs, adding to the evidence that the observed VB anion signal should not be ascribed to A9. In a condensed phase environment resembling *in vivo* conditions, the A9 VB anion might become operative through local interactions stabilizing the VB anion. The Bowen group reported photoelectron spectra of $A^-(H_2O)_{n=1-7}$ indicating that the A9 VB anion is adiabatically stable when complexed to four water molecules,[53] thereby suggesting that a DB to VB transition may become feasible in hydrated environments. A7 does show a (shallow) VB minimum, this minimum is however substantially higher in energy than that of the DB anion. Also, no evidence of a DB state with eBE ≈ 0.27 eV (corresponding to the A7 DB anion, Table I) is observed, thereby suggesting that even if A7 formation occurs in the source, it only contributes negligibly to the spectroscopic results. This renders A3 as the most plausible tautomer responsible for the observation of a bound VB anion, consistent with our assignment of the shoulder (A′) observed in the one-color spectra to I^-·A3 detachment.

Formation of the A3 VB anion could in principle result from either (a) an A9 anion reaction happening upon interaction with the laser, essentially corresponding to a concomitant tautomerization and anion transition, $A9DB \rightarrow A3VB$, and/or (b) simply an A3 anion transition, $A3DB \rightarrow A3VB$. The potential energy surfaces associated with both processes are shown in Figures 3(b) and 3(d). As is evident, the simultaneous tautomerization and anion transition mechanism (Figure 3(d)) involves a barrier of approximately 1.95 eV (45 kcal/mol), and the product is 0.28 eV (6.4 kcal/mol) higher in energy than the reactant. Furthermore, the neutral surface is only 20 meV higher in energy than the anion along the first part of the reaction pathway, and the A9 anion will therefore likely auto-detach rather than climbing the conversion barrier. However, if the reactant is A3 DB, corresponding to $A3DB \rightarrow A3VB$, the reaction is almost barrierless and overall exothermic. Concurrent with the observations in the one-color spectra, (b) appears to be the simplest explanation and primary mechanism for A3 VB anion formation. The energetically favorable A3 anion transition indicates that the A3 VB anion is capable of depleting the A3 DB anion, similar to what was observed for the anion dynamics of nitromethane.[30] This suggests that the fast decay component of the DB anion, which is mirrored by the VB anion formation, primarily is due to A3 DB anion decay. The remaining DB anion signal—more prominent at some energies than others—is thereby left to another process, most likely A9 detachment by the probe pulse. This process and the non-systematic trends observed for the DB feature are further discussed in Sec. IV C 3.

3. Dipole bound anion intensity trends and decay dynamics

The DB feature shows non-monotonic trends as a function of excitation energy with the results at 3.94 eV being a clear outlier. At this pump photon energy, the DB/VB intensity ratio is at least three times the value at the other excitation energies, the slow component of the DB anion decay is more prominent, the overall DB anion lifetime is an order of magnitude longer, and the DB anion anisotropy value is visibly more positive (Figure 6 and Table II). We hypothesize that these non-systematic trends may be due to varying contributions from the A9 and the A3 tautomers, as a result of different cluster VDEs and dipole moments localizing the DB levels at different energies. Figure 8 shows the cluster energies of I$^-$·A9 and I$^-$·A3 relative to the excitation energies; approximate energy ranges for electron capture in the electric field of the dipole of each complex are indicated as well. This diagram is based on the recognition that for molecules of same size, the binding energy of the DB anion generally increases steadily with the dipole moment,[34] being low for systems with dipole moments smaller than 2.8 D and increasing more steeply when the dipole moment exceeds 3.7 D.[33] From our recent investigation on I$^-$·uracil and I$^-$·thymine[31] and similar studies by Mabbs *et al.* on I$^-$·pyrrole,[78] it is evident that the cluster dipole moment (in contrast to the base dipole moment) determines the initial DB anion formation. The calculated cluster dipole moment of neutral I·A9 is approximately 4 D in the Franck-Condon region and decreases to 3.1 D in the relaxed geometry versus 2.5 D for the bare base, while I·A3 exhibits a vertical dipole moment of 5.6 D which is reduced slightly to 5.1 D upon relaxation (Table I), thus also enhanced relative to the bare base dipole moment of 4.7 D. As indicated in Figure 8, the larger vertical cluster dipole moment of I·A3 results in more tightly bound DB states with respect to the detachment continuum compared to I·A9.

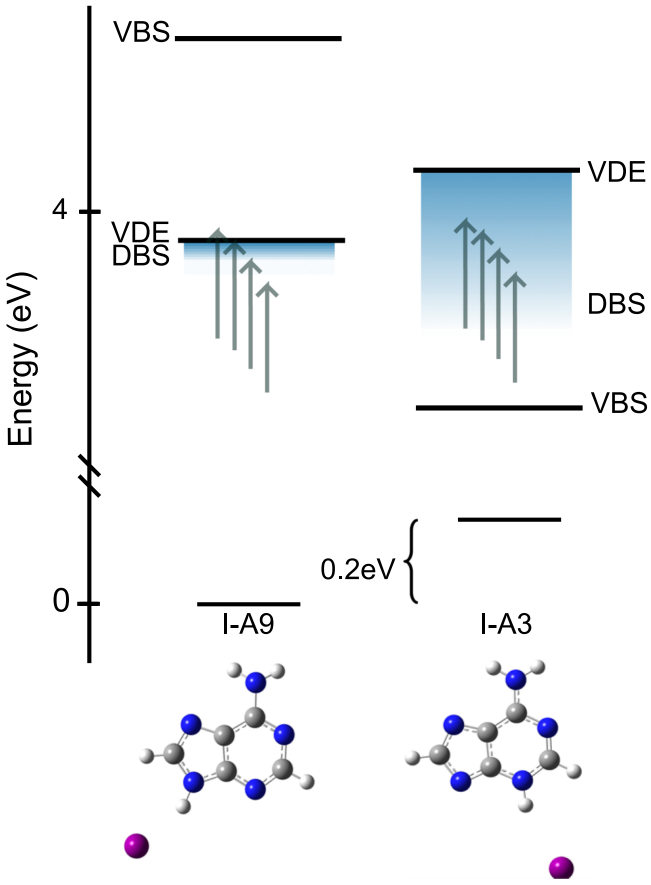

FIG. 8. Diagram of the relative energy levels and ranges for electron capture of the dipole bound states (DBS, blue shaded areas) of I$^-$·A9 and I$^-$·A3 complexes, respectively. The shaded areas are larger for I$^-$·A3 compared to I$^-$·A9 due the larger dipole moment of (I·A3)$^-$. The photon energies used in the time-resolved experiments are indicated by the grey arrows. The energy level is scaled relative to the lowest energy structure (I$^-$·A9), but the photon energies are in each case illustrated with respect to the initial state (I$^-$·A9 or I$^-$·A3).

Returning to the experimental observations, perhaps the most striking results are the intense DB feature at 3.94 eV (and somewhat at 3.97 eV) and the bi- vs. mono-exponential DB signal decay at 3.94-3.97 eV vs. 3.85-3.90 eV, respectively. Comparing these observations to Figure 8, the logical deduction is that I$^-$·A9 is prominent only at the two highest excitation energies (particularly at 3.94 eV), whereas I$^-$·A3 is in play at all energies. The I$^-$·A3 presence is implied by the fast DB signal decay component mirrored by the VB state rise observed at all photon energies. This indirectly suggests that the second, slower DB decay component—only observed at the two highest photon energies and not mirrored by any other spectral component—should be ascribed to the decay of the DB state associated with (I·A9)$^-$. The enhanced DB signal intensity at 3.94-3.97 eV compared to 3.85-3.90 eV reflects the concomitant contribution of both tautomeric complexes at the high photon energies, and the particularly strong signal at 3.94 eV is consistent with this energy being approximately resonant with the DB state of (I·A9)$^-$. Finally, the observation of the (I·A9)$^-$ tautomer in a very narrow energy region is consistent with the smaller cluster dipole moment of I·A9; at 3.94-3.97 eV, the DB state of (I·A9)$^-$ is accessible, while photon energies ≤3.90 eV are too far below the DB resonance of (I·A9)$^-$. Conversely, the DB levels of the (I·A3)$^-$ complex span a larger energy region and can be accessed by all the photon energies used.

4. Mono- and bi-exponential decay dynamics

By virtue of the apparent bi-exponential DB signal decay assigned to the separate decays of A9 and A3 DB anions, essentially both dipole- and the A3 VB anions all display mono-exponential decay dynamics. This differs from I$^-$·uracil and I$^-$·thymine, where bi-exponential decays were observed for all anionic states when examined at near VDE-excitation energies. For I$^-$·uracil and I$^-$·thymine, the bi-exponential decay was ascribed to autodetachment prior and subsequent to iodine loss. In this section, we consider the decay dynamics of the excited I$^-$·adenine complexes, and why they might differ from those observed in I$^-$·uracil and I$^-$·thymine.

In the DB state of the complex at the vertical excitation geometry, there is an attractive dipole-induced dipole interaction between adenine and the iodine atom counterbalanced by a repulsive interaction between the iodine atom and dipole-bound electron. The molecular dipole moment of A9 is considerably smaller than those of uracil and thymine (by approximately 2 D), resulting in a weaker attraction between iodine and A9 compared to uracil and thymine.[29,31] Consequently, iodine may leave the (I·A9)$^-$ complex immediately after charge transfer due to the initial repulsive I·A9 interaction as mentioned in Sec. IV C 1, while iodine adheres longer to uracil and thymine due to the stronger I·base attractive interactions. However, regardless of whether iodine leaves the A9 anion or not, the observed mono-exponential decay of the DB state suggests that the interaction between iodine and A9 does not lead to an observable effect on the decay mechanism, which most likely is statistical autodetachment. The lifetime of the $(I{\cdot}A9)^-$ DB anion drops dramatically by an order of magnitude (1 ns at 3.94 eV to 150 ps at 3.97 eV) upon a slight increase of the photon energy, demonstrating how small vibrational excitation increases the autodetachment efficiency for the loosely bound $(I{\cdot}A9)^-$ DB state.

In contrast, the $(I{\cdot}A3)^-$ DB anions are formed well below the detachment energy and can therefore not easily auto-detach. Instead, the $(I{\cdot}A3)^-$ DB anions can transition into the energetically accessible VB state, which is the only efficient decay channel consistent with the observed mono-exponential decay. This mechanism is further in accord with the decay dynamics displayed by the DB anion of nitromethane exhibiting a qualitatively similar DB vs. VB energy landscape.[30] The formation barrier is small, and efficient conversion is observed at all photon energies with the expected increased rate at higher excitation energies.

The A3 VB anion lifetime is independent of photon energy within error bars, with a constant mono-exponential lifetime of about 60-70 ps. Based on the energetics in Fig. 8, it is not obvious that there is enough available energy for autodetachment to occur, since the calculated AEA of the neutral I·A3 complex (AEA = 3.99 eV) exceeds the used photon energies. While some of the $I^-{\cdot}A$ ions may be generated in the ion source with enough vibrational excitation to enable autodetachment from the A3 VB state, one must consider whether alternate decay mechanisms are feasible. One possibility is H atom loss, leaving a deprotonated adenine anion at the N3 position. To assess this mechanism, the energy of this final state relative to the deprotonated anion at the N1 position is needed; this has not been determined, to our knowledge. Planned experiments at higher probe energies will be able to detect the production of deprotonated nucleobase anions, for which the electron binding energies are in the range of 3.5 eV.[86,87]

V. CONCLUSION

In order to gain new insights into the interaction of low energy electrons with adenine, photoexcited binary iodide-adenine anion complexes have been studied using one-color and time-resolved photoelectron imaging along with electronic structure calculations that take the three most abundant adenine tautomers into account. The experimental data showed evidence of two adenine tautomers contributing to the one-photon photoelectron spectra and the electron attachment dynamics subsequent to photoexcitation. Based on the theoretical results, these tautomers were interpreted to be the canonical A9 and the A3 tautomers. We do not observe any evidence of the A7 tautomer in either one-color or time-resolved PEI results. The main findings can be summarized as follows:

1. Photoexcitation of $I^-{\cdot}A9$ forms dipole bound anions near the VDE of the $I^-{\cdot}$ A9 complex of 3.96 eV. The energy range in which $I^-{\cdot}A9$ anions are formed is narrow compared to $I^-{\cdot}A3$, $I^-{\cdot}$uracil, and $I^-{\cdot}$thymine due to the smaller dipole moment of A9. The dipole bound anion of $I^-{\cdot}A9$ decays mono-exponentially in an autodetachment process that is significantly sped up upon slight vibrational excitation.
2. The dipole-to-valence bound anion transition in $I^-{\cdot}A9$ is energetically unfeasible and no transition was observed in the time-resolved experiments for this tautomer. Calculations find the valence bound anion of A9 to be metastable and higher in energy than the A9 neutral, consistent with the existing literature. Indications of a metastable A9 valence anion, formed upon A9 absorption and subsequent electron transfer from iodide to the empty π orbital, were observed as a shape resonance with a constant electron kinetic energy in the one-color spectra.
3. $I^-{\cdot}A3$ exhibits both dipole and valence bound anions well below the electron detachment energy of the complex (4.11 eV), and a clear dipole-to-valence transition was observed in the time-resolved experiments, as evidenced by matching decay and rise components of the spectral features for $I^-{\cdot}A3$ dipole and valence anions, respectively. The dipole-to-valence bound anion transition barrier was theoretically found to be 30 meV, and the anion conversion is overall exothermic consistent with the efficient transition observed experimentally.

This contribution complements our previous investigations on uracil, thymine, and nitromethane and show that dipole bound states can in fact act as doorway states for valence bound anion formation when the valence state is energetically accessible. The results also suggests that unless biological adenine, A9, tautomerizes into A3, adenine is less susceptible to both dipole and especially valence bound anion formation in the gas phase compared to the nucleobases uracil and thymine. When embedded in a dielectric solvent, the valence anion of biological adenine might become operative, and similar investigations on hydrated adenine are therefore highly desirable in order to increase understanding of the potential implication of dipole and valence bound anions in DNA and RNA damage under *in vivo* conditions.

ACKNOWLEDGMENTS

The work described in this paper was funded by the National Science Foundation (NSF) under Grant No. CHE-1011819. A.B.S. gratefully acknowledges support from The Villum Foundation. T.T. acknowledges support from the Ministry of Education, Culture, Sports, Science, and Technology of Japan (Grant No. 21550005).

[1] K. Aflatooni, G. A. Gallup, and P. D. Burrow, J. Phys. Chem. A **102**, 6205 (1998).
[2] M. A. Huels, I. Hahndorf, E. Illenberger, and L. Sanche, J. Chem. Phys. **108**, 1309 (1998).
[3] B. Boudaïffa, P. Cloutier, D. Hunting, M. A. Huels, and L. Sanche, Science **287**, 1658 (2000).
[4] M. A. Huels, B. Boudaïffa, P. Cloutier, D. Hunting, and L. Sanche, J. Am. Chem. Soc. **125**, 4467 (2003).
[5] G. Hanel, B. Gstir, S. Denifl, P. Scheier, M. Probst, B. Farizon, M. Farizon, E. Illenberger, and T. D. Märk, Phys. Rev. Lett. **90**, 188104 (2003).
[6] S. Denifl, S. Ptasińska, M. Probst, J. Hrusak, P. Scheier, and T. D. Märk, J. Phys. Chem. A **108**, 6562 (2004).
[7] F. Martin, P. D. Burrow, Z. L. Cai, P. Cloutier, D. Hunting, and L. Sanche, Phys. Rev. Lett. **93**, 068101 (2004).
[8] L. Sanche, Eur. Phys. J. D **35**, 367 (2005).

[9] D. Huber, M. Beikircher, S. Denifl, F. Zappa, S. Matejcik, A. Bacher, V. Grill, T. D. Märk, and P. Scheier, J. Chem. Phys. **125**, 084304 (2006).

[10] L. Sanche, Nature **461**, 358 (2009).

[11] R. Barrios, P. Skurski, and J. Simons, J. Phys. Chem. B **106**, 7991 (2002).

[12] X. Pan, P. Cloutier, D. Hunting, and L. Sanche, Phys. Rev. Lett. **90**, 208102 (2003).

[13] X. F. Li, M. D. Sevilla, and L. Sanche, J. Am. Chem. Soc. **125**, 13668 (2003).

[14] J. Berdys, I. Anusiewicz, P. Skurski, and J. Simons, J. Am. Chem. Soc. **126**, 6441 (2004).

[15] J. Simons, Acc. Chem. Res. **39**, 772 (2006).

[16] H.-Y. Chen, P.-Y. Yang, H.-F. Chen, C.-L. Kao, and L.-W. Liao, J. Phys. Chem. B **118**, 11137 (2014).

[17] X. Pan and L. Sanche, Chem. Phys. Lett. **421**, 404 (2006).

[18] S. Gohlke, H. Abdoul-Carime, and E. Illenberger, Chem. Phys. Lett. **380**, 595 (2003).

[19] H. Abdoul-Carime, S. Gohlke, and E. Illenberger, Phys. Rev. Lett. **92**, 168103 (2004).

[20] H. Abdoul-Carime, J. Langer, M. A. Huels, and E. Illenberger, Eur. Phys. J. D **35**, 399 (2005).

[21] S. Ptasińska, S. Denifl, V. Grill, T. D. Märk, E. Illenberger, and P. Scheier, Phys. Rev. Lett. **95**, 093201 (2005).

[22] S. Ptasińska, S. Denifl, V. Grill, T. D. Märk, P. Scheier, S. Gohlke, M. A. Huels, and E. Illenberger, Angew. Chem., Int. Ed. **44**, 1647 (2005).

[23] S. Ptasińska, S. Denifl, P. Scheier, E. Illenberger, and T. D. Märk, Angew. Chem., Int. Ed. **44**, 6941 (2005).

[24] J. Berdys, P. Skurski, and J. Simons, J. Phys. Chem. B **108**, 5800 (2004).

[25] A. M. Scheer, K. Aflatooni, G. A. Gallup, and P. D. Burrow, Phys. Rev. Lett. **92**, 068102 (2004).

[26] A. Kumar and M. D. Sevilla, J. Am. Chem. Soc. **130**, 2130 (2008).

[27] S. B. King, M. A. Yandell, and D. M. Neumark, Faraday Discuss. **163**, 59 (2013).

[28] M. A. Yandell, S. B. King, and D. M. Neumark, J. Am. Chem. Soc. **135**, 2128 (2013).

[29] S. B. King, M. A. Yandell, A. B. Stephansen, and D. M. Neumark, J. Chem. Phys. **141**, 224310 (2014).

[30] M. A. Yandell, S. B. King, and D. M. Neumark, J. Chem. Phys. **140**, 184317 (2014).

[31] S. B. King, A. B. Stephansen, Y. Yokoi, M. A. Yandell, A. Kunin, T. Takayanagi, and D. M. Neumark, J. Chem. Phys. **143**, 024312 (2015).

[32] O. H. Crawford, Mol. Phys. **20**, 585 (1971).

[33] G. L. Gutsev and L. Adamowicz, Chem. Phys. Lett. **235**, 377 (1995).

[34] G. L. Gutsev and L. Adamowicz, J. Phys. Chem. **99**, 13412 (1995).

[35] A. F. Jalbout and L. Adamowicz, Adv. Quantum Chem. **52**, 231 (2007).

[36] T. Sommerfeld, Phys. Chem. Chem. Phys. **4**, 2511 (2002).

[37] T. Sommerfeld, J. Chem. Phys. **126**, 124301 (2007).

[38] T. Sommerfeld, J. Phys. Chem. A **108**, 9150 (2004).

[39] H. Motegi and T. Takayanagi, J. Mol. Struct.: THEOCHEM **907**, 85 (2009).

[40] T. Takayanagi, T. Asakura, and H. Motegi, J. Phys. Chem. A **113**, 4795 (2009).

[41] F. Carelli, F. A. Gianturco, R. Wester, and M. Satta, J. Chem. Phys. **141**, 054302 (2014).

[42] F. Carelli, M. Satta, T. Grassi, and F. A. Gianturco, Astrophys. J. **774**, 97 (2013).

[43] S. Carles, F. Lecomte, J. P. Schermann, and C. Desfrançois, J. Phys. Chem. A **104**, 10662 (2000).

[44] M. Hanus, M. Kabelac, J. Rejnek, F. Ryjacek, and P. Hobza, J. Phys. Chem. B **108**, 2087 (2004).

[45] R. D. Brown, P. D. Godfrey, D. McNaughton, and A. P. Pierlot, J. Chem. Soc., Chem. Commun. **1989**, 37.

[46] N. A. Oyler and L. Adamowicz, J. Phys. Chem. **97**, 11122 (1993).

[47] M. Haranczyk, M. Gutowski, X. Li, and K. H. Bowen, Proc. Natl. Acad. Sci. U. S. A. **104**, 4804 (2007).

[48] X. Li, K. H. Bowen, M. Haranczyk, R. A. Bachorz, K. Mazurkiewicz, J. Rak, and M. Gutowski, J. Chem. Phys. **127**, 174309 (2007).

[49] E. D. Raczyńska, M. Makowski, K. Zientara-Rytter, K. Kolczyńska, T. M. Stepniewski, and M. Hallmann, J. Phys. Chem. A **117**, 1548 (2013).

[50] V. Périquet, A. Moreau, S. Carles, J. P. Schermann, and C. Desfrançois, J. Electron Spectrosc. Relat. Phenom. **106**, 141 (2000).

[51] C. Desfrançois, H. Abdoul-Carime, and J. P. Schermann, J. Chem. Phys. **104**, 7792 (1996).

[52] D. Roca-Sanjuán, M. Merchan, L. Serrano-Andres, and M. Rubio, J. Chem. Phys. **129**, 095104 (2008).

[53] S. Eustis, D. Wang, S. Lyapustina, and K. H. Bowen, J. Chem. Phys. **127**, 224309 (2007).

[54] K. Mazurkiewicz, M. Haranczyk, M. Gutowski, J. Rak, D. Radisic, S. N. Eustis, D. Wang, and K. H. Bowen, J. Am. Chem. Soc. **129**, 1216 (2007).

[55] M. L. Nugent and L. Adamowicz, Mol. Phys. **103**, 1467 (2005).

[56] M. P. Fülscher, L. Serrano-Andres, and B. O. Roos, J. Am. Chem. Soc. **119**, 6168 (1997).

[57] G. H. Roehrig, N. A. Oyler, and L. Adamowicz, J. Phys. Chem. **99**, 14285 (1995).

[58] S. Ullrich, T. Schultz, M. Z. Zgierski, and A. Stolow, Phys. Chem. Chem. Phys. **6**, 2796 (2004).

[59] C. E. Crespo-Hernandez, B. Cohen, P. M. Hare, and B. Kohler, Chem. Rev. **104**, 1977 (2004).

[60] F. Buchner, H. H. Ritze, J. Lahl, and A. Lubcke, Phys. Chem. Chem. Phys. **15**, 11402 (2013).

[61] A. V. Davis, R. Wester, A. E. Bragg, and D. M. Neumark, J. Chem. Phys. **118**, 999 (2003).

[62] A. E. Bragg, J. R. R. Verlet, A. Kammrath, O. Cheshnovsky, and D. M. Neumark, J. Am. Chem. Soc. **127**, 15283 (2005).

[63] V. Dribinski, A. Ossadtchi, V. A. Mandelshtam, and H. Reisler, Rev. Sci. Instrum. **73**, 2634 (2002).

[64] G. M. Roberts, J. L. Nixon, J. Lecointre, E. Wrede, and J. R. R. Verlet, Rev. Sci. Instrum. **80**, 053104 (2009).

[65] M. J. Frisch, G. W. Trucks, H. B. Schlegel, G. E. Scuseria, M. A. Robb, J. R. Cheeseman, G. Scalmani, V. Barone, B. Mennucci, G. A. Petersson, H. Nakatsuji, M. Caricato, X. Li, H. P. Hratchian, A. F. Izmaylov, J. Bloino, G. Zheng, J. L. Sonnenberg, M. Hada, M. Ehara, K. Toyota, R. Fukuda, J. Hasegawa, M. Ishida, T. Nakajima, Y. Honda, O. Kitao, H. Nakai, T. Vreven, J. A. Montgomery, Jr., J. E. Peralta, F. Ogliaro, M. Bearpark, J. J. Heyd, E. Brothers, K. N. Kudin, V. N. Staroverov, R. Kobayashi, J. Normand, K. Raghavachari, A. Rendell, J. C. Burant, S. S. Iyengar, J. Tomasi, M. Cossi, N. Rega, J. M. Millam, M. Klene, J. E. Knox, J. B. Cross, V. Bakken, C. Adamo, J. Jaramillo, R. Gomperts, R. E. Stratmann, O. Yazyev, A. J. Austin, R. Cammi, C. Pomelli, J. W. Ochterski, R. L. Martin, K. Morokuma, V. G. Zakrzewski, G. A. Voth, P. Salvador, J. J. Dannenberg, S. Dapprich, A. D. Daniels, Ö. Farkas, J. B. Foresman, J. V. Ortiz, J. Cioslowski, and D. J. Fox, GAUSSIAN 09, Gaussian, Inc., Wallingford, CT, 2009.

[66] K. A. Peterson, B. C. Shepler, D. Figgen, and H. Stoll, J. Phys. Chem. A **110**, 13877 (2006).

[67] J. Simons, J. Phys. Chem. A **112**, 6401 (2008).

[68] Y. Yokoi, K. Kano, Y. Minoshima, and T. Takayanagi, Comput. Theor. Chem. **1046**, 99 (2014).

[69] L. M. Salter and G. M. Chaban, J. Phys. Chem. A **106**, 4251 (2002).

[70] H. Hotop, M. W. Ruf, M. Allan, and I. I. Fabrikant, in *Advances in Atomic, Molecular, and Optical Physics*, edited by B. Bederson and H. Walther (Academic Press, 2003), p. 85.

[71] S. Tonzani and C. H. Greene, J. Chem. Phys. **124**, 054312 (2006).

[72] C. Winstead and V. McKoy, J. Chem. Phys. **125**, 244302 (2006).

[73] Y.-F. Wang and S. X. Tian, Phys. Chem. Chem. Phys. **13**, 6169 (2011).

[74] K. L. Reid, Annu. Rev. Phys. Chem. **54**, 397 (2003).

[75] J. H. Hendricks, S. A. Lyapustina, H. L. de Clercq, and K. H. Bowen, J. Chem. Phys. **108**, 8 (1998).

[76] C. R. S. Mooney, D. A. Horke, A. S. Chatterley, A. Simperler, H. H. Fielding, and J. R. R. Verlet, Chem. Sci. **4**, 921 (2013).

[77] M. H. Elkins, H. L. Williams, and D. M. Neumark, J. Chem. Phys. **142**, 234501 (2015).

[78] R. Mabbs, E. Surber, and A. Sanov, J. Chem. Phys. **122**, 054308 (2005).

[79] R. D. Brown, P. D. Godfrey, D. McNaughton, and A. P. Pierlot, Chem. Phys. Lett. **156**, 61 (1989).

[80] C. Plützer and K. Kleinermanns, Phys. Chem. Chem. Phys. **4**, 4877 (2002).

[81] S. K. Mishra, M. K. Shukla, and P. C. Mishra, Spectrochim. Acta, Part A **56**, 1355 (2000).

[82] C. Z. Bisgaard, H. Satzger, S. Ullrich, and A. Stolow, ChemPhysChem **10**, 101 (2009).

[83] R. N. Compton, H. S. Carman, C. Desfrançois, H. Abdoul-Carime, J. P. Schermann, J. H. Hendricks, S. A. Lyapustina, and K. H. Bowen, J. Chem. Phys. **105**, 3472 (1996).

[84] F. Lecomte, S. Carles, C. Desfrançois, and M. A. Johnson, J. Chem. Phys. **113**, 10973 (2000).

[85] C. E. H. Dessent, J. Kim, and M. A. Johnson, Faraday Discuss. **115**, 395 (2000).

[86] B. F. Parsons, S. M. Sheehan, T. A. Yen, D. M. Neumark, N. Wehres, and R. Weinkauf, Phys. Chem. Chem. Phys. **9**, 3291 (2007).

[87] D. L. Huang, H. T. Liu, C. G. Ning, G. Z. Zhu, and L. S. Wang, Chem. Sci. **6**, 3129 (2015).